ACS APPLIED MATERIALS & INTERFACES

www.acsami.org

Research Article

Formation of a 2D Meta-stable Oxide by Differential Oxidation of AgCu Alloys

Kevin Schweinar,* Sebastian Beeg, Caroline Hartwig, Catherine R. Rajamathi, Olga Kasian, Simone Piccinin, Mauricio J. Prieto, Liviu C. Tanase, Daniel M. Gottlob, Thomas Schmidt, Dierk Raabe, Robert Schlögl, Baptiste Gault, Travis E. Jones, and Mark T. Greiner*

Cite This: *ACS Appl. Mater. Interfaces* 2020, 12, 23595−23605

Read Online

ACCESS | Metrics & More | Article Recommendations | Supporting Information

ABSTRACT: Metal alloy catalysts can develop complex surface structures when exposed to reactive atmospheres. The structures of the resulting surfaces have intricate relationships with a myriad of factors, such as the affinity of the individual alloying elements to the components of the gas atmosphere and the bond strengths of the multitude of low-energy surface compounds that can be formed. Identifying the atomic structure of such surfaces is a prerequisite for establishing structure−property relationships, as well as for modeling such catalysts in ab initio calculations. Here, we show that an alloy, consisting of an oxophilic metal (Cu) diluted into a noble metal (Ag), forms a meta-stable two-dimensional oxide monolayer, when the alloy is subjected to oxidative reaction conditions. The presence of this oxide is correlated with selectivity in the corresponding test reaction of ethylene epoxidation. In the present study, using a combination of in situ, ex situ, and theoretical methods (NAP-XPS, XPEEM, LEED, and DFT), we determine the structure to be a two-dimensional analogue of Cu_2O, resembling a single lattice plane of Cu_2O. The overlayer holds a pseudo-epitaxial relationship with the underlying noble metal. Spectroscopic evidence shows that the oxide's electronic structure is qualitatively distinct from its three-dimensional counterpart, and because of weak electronic coupling with the underlying noble metal, it exhibits metallic properties. These findings provide precise details of this peculiar structure and valuable insights into how alloying can enhance catalytic properties.

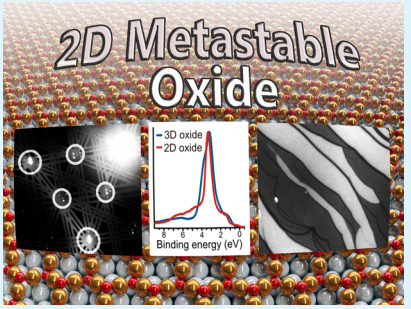

KEYWORDS: *oxide monolayer, dilute alloy, meta-stable, XPS, 2-dimensional material*

1. INTRODUCTION

1.1. Overview. One major difficulty in contemporary catalysis research is bridging the so-called "complexity gap". The complexity gap refers to the fact that catalysts used in applications of interest are much more complex entities than the model systems for which we are able to obtain precise atomic-scale detail in fundamental studies. For instance, subjecting a material to the conditions of industrial catalysts can give rise to the formation of a multitude of chemical phases, any of which could potentially play a role in catalysis, but remain unknown to us from model investigations. In order to accurately model catalysts in reactive conditions—for instance, to calculate adsorption energies and reaction barriers for use in micro-kinetic simulations—we require accurate knowledge of surface structures present in reaction conditions.

Much progress has been made in recent years to bridge the complexity gap, with the development of numerous in situ characterization methods. Unfortunately, it is often the case that one must sacrifice precision for in situ measurements. For instance, commonly used near-ambient pressure X-ray photoelectron spectroscopy (XPS) setups probe tens to hundreds of square microns of the sample surface to maximize the signal-to-noise ratio. However, the collected signal reflects an average of the probed area, which in turn prevents the spatial differentiation and unequivocal identification of localized phases. Consequently, one is often left with uncertain and ambiguous information about one's sample. In the present work, we bridge part of the complexity gap by combining several in situ, ex situ, and theoretical methods to identify a unique structure that forms on an alloy in a reactive gas atmosphere.

Metal alloys hold potential for developing novel catalysts. Under reaction conditions, synergies can arise between alloying elements to result in improved catalytic properties compared to the pure constituent metals. Heating an alloy in a reactive gas atmosphere can result in surface restructuring, phase segregation, preferential oxidation, and the formation of unique surface-adsorbate superstructures. Much theoretical effort has been devoted to predicting which alloy compositions

Received: March 5, 2020
Accepted: April 21, 2020
Published: April 21, 2020

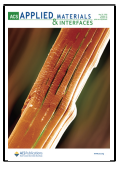

exhibit enhanced catalytic properties;[1,2] however, without knowledge of the structures formed when exposing an alloy to reaction conditions, one is likely to overlook some important aspects.

A common strategy for predicting surface structures in reactive atmospheres is to propose candidate structures and use ab-initio thermodynamics to calculate their stabilities in a given atmosphere.[3] The greatest difficulty here is choosing the candidate structures because the configurational space of all possible structures is far too large to test them all. Typical approaches for choosing candidate structures include a "chemical intuition", where one selects structural motifs known to exist from X-ray diffraction data or ultra-high vacuum surface science studies. Another approach is to generate candidate structures using genetic algorithms. In any case, there is no guarantee that the true surface structure was among the candidate structures tested, and experimental verification is the only way to determine which structures actually form, making such data extremely valuable for reaction pathway calculations.

Here, we take a closer look at a bimetallic alloy, consisting of an oxophilic metal (Cu) and a noble metal (Ag). In particular, we assess the (electronic) structure of the surface oxide that forms, when the alloy is exposed to an oxygen-containing reaction atmosphere. Previous reports have shown that the oxophilic element diffuses to the surface to form an unknown oxidic surface structure that is correlated with selectivity for the epoxidation reaction.[4−6] In this contribution, we employ a suite of in situ techniques, with pressures ranging from 10^{-1} to 10^{-5} mbar. We show how it is possible to bridge part of the *complexity gap* by linking several datasets through shared attributes. The approach involves (1) characterizing spectroscopic properties using near-ambient pressure XPS (NAP-XPS) and near edge X-ray absorption fine structure (NEXAFS) measurements; (2) identifying spectroscopic fingerprints that are correlated with epoxide selectivity; (3) characterizing the structure by means of X-ray photoemission electron microscopy (XPEEM) and low-energy electron diffraction (LEED), and verifying that the spectroscopic fingerprints observed under in situ NAP conditions, are also observed under XPEEM conditions; and (4) comparing the measured structural and spectroscopic data with simulated data from the candidate structures.

Using this approach, we determine the previously found mystery phase as a two-dimensional meta-stable Cu-oxide, structurally analogous to a single lattice plane of Cu_2O, as depicted in Figure 1. Our findings provide valuable insights into the kinds of structures that can form on alloy catalysts.

2. MATERIALS AND METHODS

2.1. Experimental Section. Environmental scanning electron microscopy (ESEM) experiments were performed in a FEI Quanta 200 FEG, using a differentially pumped lens column and a gaseous secondary electron detector. Gases were continually flowed into the chamber via mass flow controllers to a pressure of 0.3 mbar. Sample heating was accomplished through an infrared laser fed into the chamber via a fiber-optics feed-through.

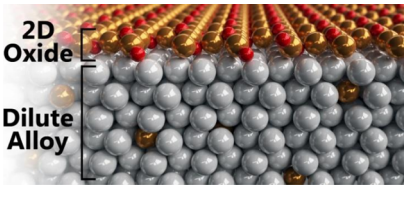

Figure 1. Rendition of the Cu_xO_y structure formed on AgCu in oxidizing environments.

In situ NAP-XPS measurements were performed at the ISISS beamline at the synchrotron radiation facility BESSY II of the Helmholtz−Zentrum Berlin (HZB), using a differentially pumped Phoibos 150 hemispherical analyzer from Specs GmbH. The ISISS beamline is a dipole photon source, with a plane-grating monochromator, delivering 6×10^{10} photons/s/0.1 A and an energy resolution of >15 000 at 400 eV. NAP-XPS experiments were performed in a gas pressure of 0.3 mbar. Ethylene epoxidation conditions utilized a 1:1 mixture of O_2/C_2H_4 with a total flow rate of 6 mL/min. Sample heating up to 250 °C was accomplished by illuminating the backside of the sample pellets with an infrared laser. The sample pellets were prepared following the procedure reported in ref 4. This experiment yields nonspatially resolved XPS (Cu 2p, O 1s, Ag 3d), NEXAFS (O K, Cu L), and valence band spectra under conditions where ethylene epoxide is formed.

Low-energy electron microscopy (LEEM)/LEED and XPEEM measurements were carried out in the SMART spectro-microscope operating at the UE49-PGM beamline at the synchrotron radiation facility BESSY II of the HZB. The aberration-corrected and energy-filtered LEEM/PEEM instrument combines microscopy, diffraction, and spectroscopy techniques for comprehensive characterization. The instrument achieves an experimentally demonstrated lateral resolution of 2.6 nm in LEEM and 18 nm in energy-filtered XPEEM mode, respectively.[7,8]

We used a polycrystalline AgCu diffusion couple for our first experiment. The sample was prepared by fusing together a piece of high purity silver and copper. This couple was then annealed in Ar for 21 h at 750 °C before it was cut and mechanically ion polished. A single crystalline AgCu(111) surface was used for the second XPEEM experiment.

The AgCu(111) crystal was prepared by depositing a copper thin film of 50 nm thickness onto a Ag(111) crystal by physical vapor deposition. The crystal was then annealed in H_2 inside a lab-source NAP-XPS system at temperatures from 100 to 630 °C while monitoring the Cu 2p signal (see Supporting Information S.1) and then annealed in H_2 at 550 °C for additional 4 h. The annealing procedure leads to Cu reduction and diffusion into the Ag(111) crystal.

The single crystal was transported in air from Mülheim an der Ruhr, Germany, to Berlin, Germany, one day after the annealing treatment. After loading the sample into the XPEEM microscope at the SMART beamline, the sample was sputtered with Ar^+ (1.5 keV ion energy, 0.06 μA flux, for 15 min) and annealed in UHV (3×10^{-9} mbar) for 5 min at 400 °C. Following this procedure, the surface of the sample was crystalline, but too rough for high-resolution imaging (see Supporting Information S.2-A). The sputter-annealing treatment was repeated 23 times until a contaminant-free and smooth surface was obtained (see S.2-B). The surface was then reduced by heating to 400 °C in 1×10^{-5} mbar H_2 for 10 min. This resulted in a clean surface, free of oxidized copper species. The oxidation of the alloy was performed in 1×10^{-5} mbar O_2 at 300 °C. These experiments yield spatially resolved XPS (O 1s, Cu 2p, Ag 3d), valence band spectra, microscopy images, and LEED patterns.

NAP-XPS measurements on the AgCu(111) single crystal were performed under identical conditions as the XPEEM experiments, prepared as described above. The measurements were carried out at the BelChem beamline of the synchrotron radiation facility BESSY II of the HZB, using a differentially pumped Phoibos 150 hemispherical analyzer from Specs GmbH. The results from this method provide high quality and energy calibrated non-spatially resolved XPS (Cu 2p, O 1s, Ag 3d), Auger spectra (Cu LMM), NEXAFS (O K, Cu L), and valence band spectra.

The density functional theory (DFT) calculations were performed using the Heyd−Scuseria−Ernzerhof HSE06 exchange and correlation functional.[9] We used optimized norm-conserving Vanderbilt

https://dx.doi.org/10.1021/acsami.0c03963
ACS Appl. Mater. Interfaces 2020, 12, 23595−23605

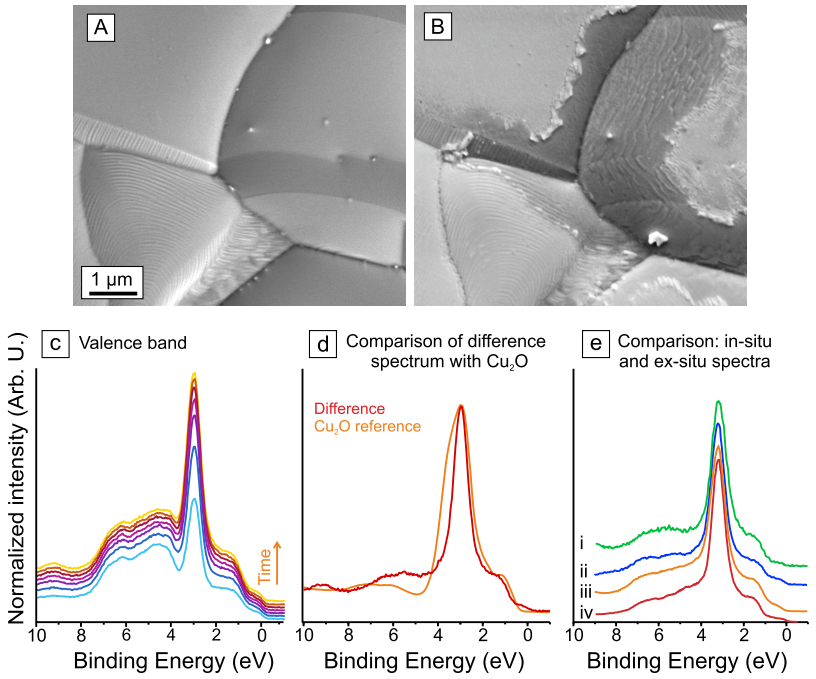

Figure 2. ESEM images of (A) a reduced AgCu foil (0.5 at. % Cu) and (B) the same foil while heated in 0.3 mbar ethylene and oxygen at 300 °C. (C) In situ NAP-XPS valence spectra ($h\nu$ = 150 eV) measured as a time series under epoxidation conditions (time step = 50 min, 0.3 mbar, 1:1 O_2/C_2H_4, 300 C). (D) Comparison of a difference spectrum generated (see Supporting Information for details) with a reference spectrum of Cu_2O. (E) Comparison of several in situ measurements, using a Phoibos NAP-150 analyzer (i–iii) with a measurement performed in ultra-high-vacuum, using an XPEEM analyzer (iv). Spectra i and ii are measured in 0.5 mbar of a 1:1 mixture of ethylene and oxygen. Spectrum (iii) is measured in 0.5 mbar of a dilute–O_2 mixture containing 1:50 mixture of oxygen to ethylene. Spectrum (iv) is measured on a AgCu(111) single crystal at 300 °C in 1 × 10^{-5} mbar O_2.

(ONCV), with a plane wave cutoff of 60 Ry. The surface oxides were formed on top of a Ag(111) surface, modelled using a 4-layer slab, sampling the Brillouin zone with *K*-point grids equivalent to a 12 × 12 × 1 on the 1 × 1 surface unit cell and broadening the Fermi surface using the Marzari–Vanderbilt scheme with a 0.04 Ry smearing energy. During the structural optimizations, the bottom two layers of the Ag slabs were kept fixed to bulk atomic positions. The starting geometries were taken from the work of Piccinin et al.[10] and further optimized, until forces were smaller than 0.026 eV/Å. All the calculations were performed with the Quantum ESPRESSO code.[11] The DFT calculations provide candidate structures, their energies, the density of states (DOS), and symmetry.

Each type of experiment provides a set of useful attributes that can be utilized to link the experiments together. A connectivity graph of the various kinds of data is provided in the Supporting Information (S.3). While the valence band, for instance, is an attribute that all experiments have in common, that is, that could be measured or calculated in every experiment, XPEEM, DFT, and NAP-XPS on the single crystal share the same experimental conditions. Figure S3H shows the complete connectivity graph in which the line thickness represents the number of links that exists between the different experiments. By networking commonly observed data sets among different experiments, drawing a link between atomic structure of the investigated surface oxide and its function becomes possible.

2.2. Data Analysis. Spectromicroscopy stacks were generally measured by (1) choosing a fixed photon energy, (2) setting the microscope lens settings such that the surface image plane is focused on the 2D detector, (3) band-pass filtering the photoelectrons by kinetic energy, and (4) scanning the sample potential at fixed filter settings, while measuring the resulting 2D detector image. The result of this measurement is a stack of detector images, where each image represents the spatial distribution of photoelectrons having a given binding energy, as defined by the sample potential referring to the fixed band center used for the energy filter in the given image. An alternative way to view the data is a 2D array of photoemission spectra. The (uncropped) image size is 1600 × 1200 pixels, so that there are 1.92 × 10^6 photoemission spectra in a dataset. The detector pixels were binned to make images of 400 × 300 pixels. To identify how many chemical components were present in the image stack, we performed principle component analysis (PCA) and determined how many abstract factors were significant in relation to the image noise. After this procedure, we imaged regions appearing to be phase pure and generated basis vectors by summing the spectra in these homogeneous regions. These basis vectors were then used to fit the original 120 000 spectra using linear least-squares regression, to give the result of a spatial map of the chosen basis vectors. Such maps are shown in Figures 3c,d, 4c,d, and 5a.

The XPS spectra were measured using the XPEEM instrument (SMART spectro-microscope) at the UE49-PGM beamline. They were measured by (1) choosing a photon energy, (2) in the LEEM mode, moving the sample such that the field-of-view is homogeneously covered by a single phase, and (3) setting the lenses such that the energy-dispersive plane is imaged onto the 2D detector. The resulting detector image represents binding energy (kinetic energy) along one direction and spatial dispersion along the perpendicular direction. A flat-field image was used to correct the variation in sensitivity across the detector. The spectra were summed along the spatial dispersive direction to give rise to a typical photoemission spectrum. This procedure was used for the spectra in Figures 3b, 4b, 5e,f, and Figure 10a.

The XPS spectra measured in near-ambient pressure conditions (at the BelChem beamline) were measured using a Specs GmbH Phoibos 150-NAP analyzer. In this process, (1) the photon energy was chosen, (2) the photon energy is calibrated by measuring the Fermi level, (3) electrons pass through a hemispherical analyzer holding a constant pass energy, thereby acting as a band-pass filter for electrons, (4) the photoelectrons strike a 140-channel 1D delay-line detector at the end of the hemisphere, (5) the kinetic energy of incoming electrons is ramped using a retarding potential, in the standard fixed-analyzer-transmission mode, and (6) the detector channel representing count

https://dx.doi.org/10.1021/acsami.0c03963
ACS Appl. Mater. Interfaces 2020, 12, 23595–23605

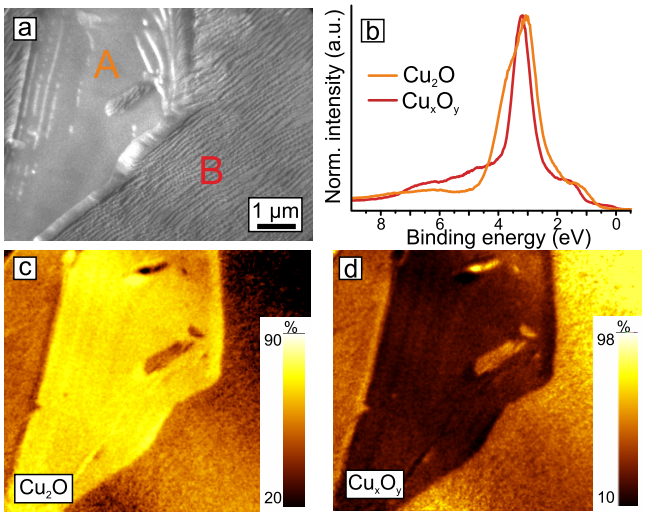

Figure 3. (a) LEEM image showing the coexistence of Cu_2O (A) and Cu_xO_y (B) on a polycrystalline AgCu sample (E_{kin} = 4.8 eV). (b) Valence band spectra ($h\nu$ = 170) of regions A and B. (c,d) Spatial distributions of Cu_2O and Cu_xO_y valence spectra, as determined from a XPEEM image stack.

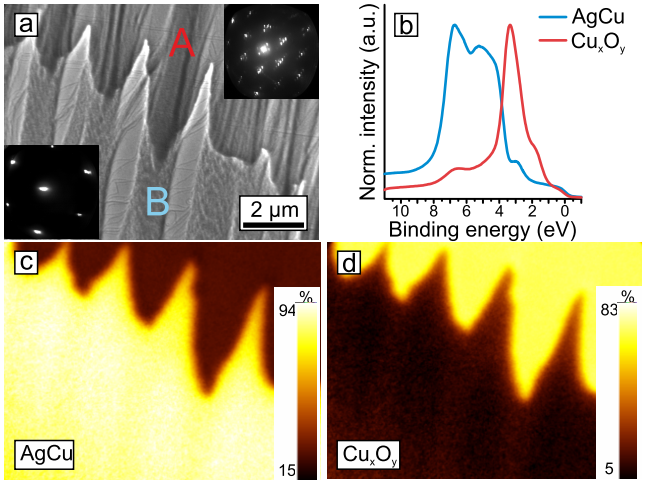

Figure 4. (a) LEEM image of a surface partially covered by Cu_xO_y (region A), E_{kin} = 5 eV. The insets show the corresponding LEED patterns at E_{kin} = 42 eV. (b) Valence spectra from regions A and B in ($h\nu$ = 170 eV). (c,d) Spatial distributions of AgCu and Cu_xO_y valence spectra, as determined from a XPEEM image stack.

rates for electrons having same kinetic energies are binned together. Such measurements result in XPS spectra as shown in Figures 2c,d,e, 5e,f, and 7.

The NEXAFS spectra were measured at the BelChem beamline. The spectra were measured by (1) scanning the photon energy across some range and (2) measuring the total electron yield by measuring the drain current at the nozzle of a Specs GmbH Phoibos 150-NAP analyzer, positioned 1 mm away from the sample surface.

3. RESULTS

3.1. Linking NAP-XPS with XPEEM. The AgCu alloy (0.5 at. % Cu) was first characterized using NAP-XPS and ESEM at conditions where ethylene epoxidation can occur (i.e. in a 1:1 mixture of ethylene and O_2, at 300 °C). Under these conditions, silver oxides are not stable, while copper oxides are,[4,10,12] and consequently, Cu becomes preferentially oxidized, forming Cu-containing oxides at the surface. For

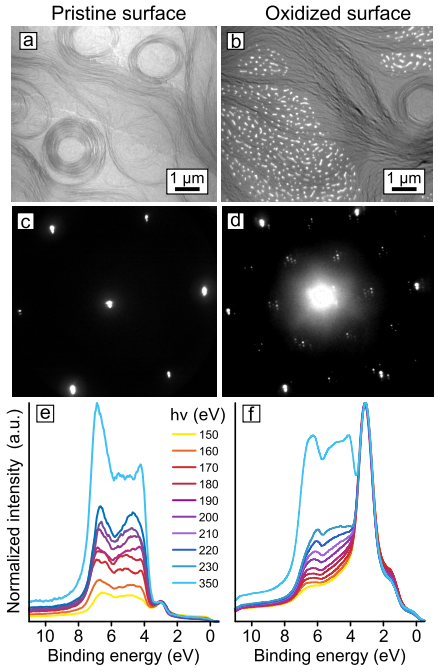

Figure 5. Comparison of the pristine (left column) and oxidized (right column) AgCu(111) surface. (a–c) LEEM image (E_{kin} = 42 eV), LEED pattern (E_{kin} = 42 eV), and (d–f) valence spectra at photon energies close to the Cooper minimum of Ag 4d.

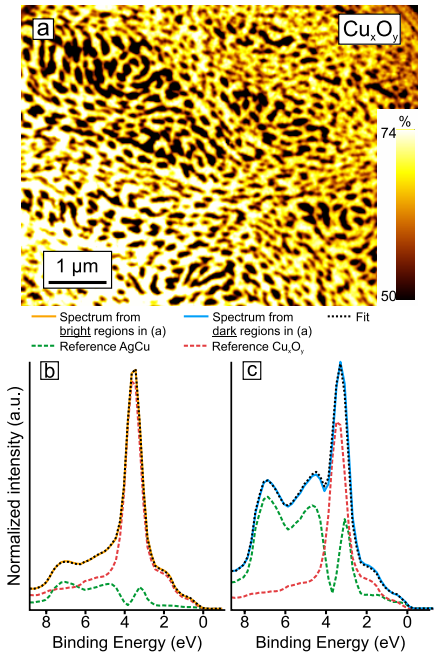

Figure 6. (a) Analyzed XPEEM valence band maps measured in $p(O_2) = 1 \times 10^{-5}$ mbar and 300 °C at a photon energy of $h\nu$ = 170 eV. The map shows the spatial distribution of Cu_xO_y. The color scale represents the percentage of the reference spectrum used to fit the map. The corresponding summed spectra of the bright colored and dark colored regions in (a) are shown in (b,c). Two components (i.e., reference metallic AgCu and reference Cu_xO_y spectrum) are required to fit the data.

instance, Figure 2 shows ESEM images of a polycrystalline AgCu foil (0.5 at. % Cu) prior to (Figure 2A) and during (Figure 2B) ethylene epoxidation (conditions are 1:1 C_2H_4/O_2, P_{tot} = 0.3 mbar at 300 °C). One can see that, during

https://dx.doi.org/10.1021/acsami.0c03963
ACS Appl. Mater. Interfaces 2020, 12, 23595−23605

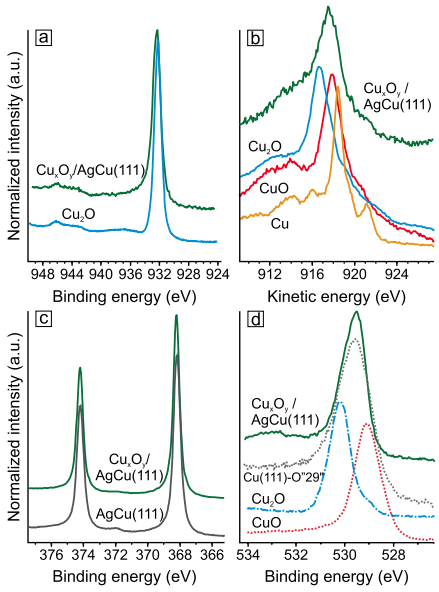

Figure 7. Comparison of photoemission spectra from Cu_xO_y/AgCu(111) with reference spectra. (a) Cu 2p core level spectra. (b) Cu LMM Auger spectra. (c) Ag $3d_{5/2}$ spectra and (d) O 1s spectra.

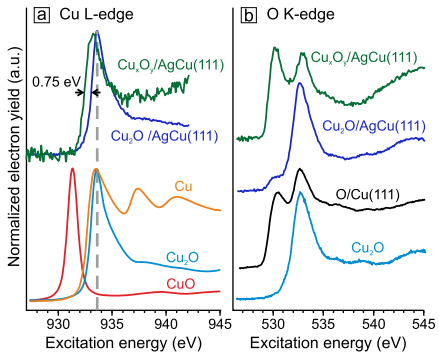

Figure 8. Experimental NEXAFS spectra of the Cu L-edge (a) and O K-edge (b) and reference spectra of similar structures [Cu, Cu_2O, CuO, and O/Cu(111)]. The spectra containing Cu_xO_y/AgCu(111) were measured in an oxidizing atmosphere (1×10^{-5} mbar O_2, 300 °C).

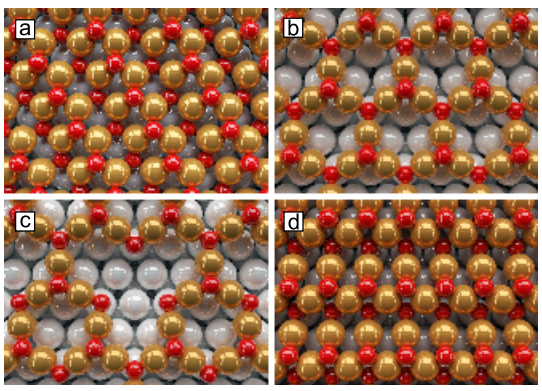

Figure 9. 3D models of proposed structured candidates. (a) Chemisorbed oxygen (Cu_4O_4), (b) p2, (c) p4, and (d) CuO-1ML.

ethylene epoxidation, the surface becomes decorated with a variety of different copper-containing oxides, as evident from the various island morphologies and changes in contrast in Figure 2B (EDX maps are provided in Figure S17).

In situ valence band photoemission spectra (Figure 2C–E) give an indication of the identities of the oxides present on the surface. The valence band spectra reflect the electronic structure of a material (particularly, the occupied DOS) and can be used as a fingerprint to distinguish CuO, Cu_2O, and metallic Ag.[13,14] The valence band spectra of AgCu in epoxidation conditions (Figure 2C) show a signal that is a linear combination of several distinct valence band fingerprints. From a multivariate analysis of the spectrum stack in Figure 2C, we find that the spectra are composed of spectra from several species (see analysis in Supporting Information), including a metallic AgCu signal and some unidentified species with a line shape similar but distinct from Cu_2O, as shown in Figure 2D. This species was previously shown to be correlated with epoxide selectivity.[4] Figure 2D shows the spectrum of this unknown species after subtracting a portion of metal Ag signal from the mixed-signal spectrum. The resulting difference spectrum is plotted with a reference spectrum of Cu_2O and exhibits distinct differences in line shape and position. These observations imply that a species is present on the surface, having an electronic structure similar to that of Cu_2O.

This information alone is not sufficient to determine the atomic structure of the unknown phase. To identify the phase, one needs to isolate it. However, the feature sizes of this phase are on the order of hundreds of nanometers (Figure 2B). To obtain a phase pure spectral signature, one requires spectroscopic methods with nanometer spatial resolution. To this end, we utilized XPEEM, with which one can obtain photoelectron spectra with a spatial resolution of ca. 20 nm. Unfortunately, this method is not capable of measurements under the same conditions as NAP-XPS; so one must first verify that the signatures observed in NAP-XPS are also present under the conditions of XPEEM measurements.

As shown in Figure 2E, the spectroscopic features observed in situ could also be produced ex situ by heating a sputter-cleaned alloy surface in 10^{-5} mbar O_2. Figure 2E shows several examples of the oxide formed in situ, including (i) an $Ag_{99.5}Cu_{0.5}$ sample at 350 °C in 0.5 mbar mixture of 1:1 O_2/C_2H_4, (ii) an $Ag_{98}Cu_2$ sample at 350 °C in 0.5 mbar mixture of 1:1 O_2/C_2H_4, and (iii) an $Ag_{99.5}Cu_{0.5}$ sample at 350 °C in a 1:50 mixture of O_2/C_2H_4.

Figure 3 shows a LEEM image and XPEEM maps of a polycrystalline AgCu alloy after oxidation in 10^{-5} mbar O_2. These images show a region of the surface where both Cu_2O and the unknown phase are present. The Cu_2O region is the island in the left half of the image (labeled A), as determined using spectro-microscopy image stacks. The image stacks represent a spatial map of the valence band spectra (measured using $h\nu$ = 150 eV). The spectra extracted from the Cu_2O region and unknown-phase region are shown in Figure 3b. These spectra were obtained by restricting the area-of-interest (AOI) of the spectrometer by using a field aperture, such that a single phase covers the entire AOI, and then measuring an XPS spectrum. Figure 3c,d shows the spatial distribution of the two valence spectra (Cu_2O and Cu_xO_y). The data processing methods are explained in the Materials and Methods section.

The beauty of this data set is that the unknown structure and the reference structure (Cu_2O) are both present in the same field of view, such that Cu_2O acts as an internal standard. With this configuration, the subtle spectroscopic differences can be very accurately compared. We can see that the difference in

https://dx.doi.org/10.1021/acsami.0c03963
ACS Appl. Mater. Interfaces 2020, 12, 23595−23605

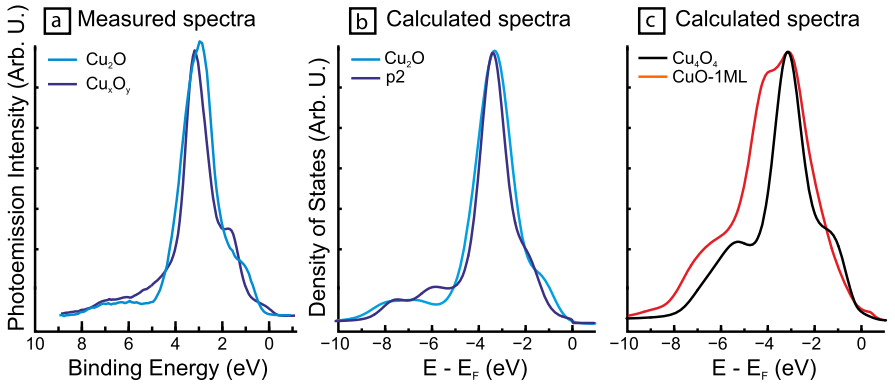

Figure 10. Comparison of (a) experimental valence band spectra of Cu_2O (internal standard) and Cu_xO_y measured at $h\nu$ = 170 eV and (b + c) DFT calculated DOS, weighted by their photoionization cross sections at 170 eV, of Cu_2O and the proposed structure candidates.

line shapes between Cu_2O and the unknown phase observed under XPEEM conditions is qualitatively the same as what was observed during the NAP-XPS measurements (see Figure 2E), suggesting that the phases formed in NAP-XPS were also stable in the XPEEM instrument. From here on, we will refer to the unknown phase as Cu_xO_y.

The polycrystalline alloy surface oxidizes non-homogeneously, with the Cu_xO_y phase covering large proportions (several tens of micrometers wide) of the surface, with the occasional appearance of Cu_2O islands, typically similar in size to that shown in Figure 3. Through exploration of the surface, we found regions where no oxidation had occurred, and the surface was still metallic. Figure 4a shows a LEEM image of such a region. Here, the Cu_xO_y surface phase terminates, and the metallic AgCu surface is exposed.

The valence spectra in Figure 4b clearly show the different valence structures of the two regions. The red and blue curves in Figure 4b are the valence spectra from the regions labeled in Figure 4a as A and B, respectively. Figure 4c,d show the spatial distributions of the two valence spectra, illustrating that region A is the Cu_xO_y phase, and region B is the non-oxidized AgCu surface. LEED patterns of these regions reveal that the AgCu surface has a (111) termination, and the Cu_xO_y has a pseudo-(2 × 2) superstructure on the (111) termination. Here, we use the prefix "pseudo" because, on close examination of the diffraction spots, one can distinguish a Moiré pattern, implying the overlayer's lattice parameter is either slightly larger or slightly smaller than that of the underlying metal lattice. A structural model for the surface is discussed in detail in Section 4.3.

3.2. Examination of AgCu(111). To better understand the structure of the Cu_xO_y surface phase, we repeated the XPEEM measurements with a AgCu(111) single crystal. Using a single crystalline sample ensures more controlled sample conditions and avoids effects related to grain boundaries. The Ag(111) single crystal contained ca. 0.7 at. % Cu, as determined by a laboratory-based XPS (see Figure S1). Here we compare the LEEM, LEED, and valence spectra of the pristine AgCu(111) surface (after 23 consecutive sputter-annealing cycles) with the same surface after oxidizing the sample in 1 × 10^{-5} mbar O_2 at 300 °C for 1 h inside the XPEEM analysis chamber.

As seen in the LEEM image in Figure 5a, the pristine AgCu(111) surface was relatively homogeneous, with flat terraces 1−2 μm wide, with mono-atomic steps discernible as very fine lines on the terraces. The LEEM image after oxidation shows strong contrast, with localized bright features on the order of ∼100 nm in diameter covering the surface. As explained further with Figure 6, the bright features are metallic AgCu, and the dark features are Cu_xO_y. These observations imply that a discontinuous mesh-like oxidic structure had formed over the surface.

From the LEED patterns in Figure 5c−d, one can clearly identify the three-fold symmetry of the pristine (111) oriented crystal. After oxidation, the LEED pattern shows a pseudo-(2 × 2) periodicity with respect to the Ag(111) surface, similar to the observation made on the oxidized polycrystalline AgCu alloy, shown in Figure 4a.

The valence spectra of the pristine and oxidized surfaces are shown in Figure 5e,f. Here, we measured a series of valence spectra using several photon energies spanning the Cooper minimum of the Ag 4d states (i.e. photon energies from 150 to 230 and 350 eV). By observing how the relative intensities change with photon energy, one can identify which features are from Ag. The valence spectra in Figure 5e,f are normalized with respect to the intensity of the Cu 3d peak (at ca. 3 eV). In the case of the pristine surface, the Ag 4d states (at ca. 4−8 eV) increase relative to the Cu 3d states for photon energies away from the Cooper minimum. The spectra also show the absence of O-related peaks (which would be at 2 eV) at photon energies that are very sensitive to O 2p states (i.e. at $h\nu$ = 150 eV). These observations imply that the surface was metallic and contained only Ag and Cu within the field of view.

In contrast, the valence spectra of the oxidized surface are dominated by the Cu 3d- and O 2p-based features, with the Ag 4d features having a substantial intensity only at photon energies far from the Cooper minimum. The line-shape of the spectrum at $h\nu$ = 150 eV is essentially the same as that observed under near-ambient pressure conditions using the same photon energy (Figure 2C).

A XPEEM spectromicroscopy map of the valence region was used to identify the spatial features seen in the LEEM image of the oxidized surface. Figure 6a shows the mapping of the Cu_xO_y spectrum. Figure 6b−c shows spectra extracted from various regions of the map. A PCA of the 120 000 spectra in the image stack showed that only two factors (i.e. spectroscopic entities/reference spectra) are required to adequately fit the experimental data through a linear combination of those factors. While PCA can indicate how many components are needed to fit the data, it cannot reveal what those components are. Thus, a subjective method was used to decide which spectra to use as reference spectra (i.e.

https://dx.doi.org/10.1021/acsami.0c03963
ACS Appl. Mater. Interfaces 2020, 12, 23595−23605

basis vectors) to fit the measured spectra. The selected internal reference spectra correspond to metallic AgCu and Cu_xO_y, as shown in Figure 6b–c. The orange spectrum in Figure 6b represents the sum of all spectra extracted from the bright-colored regions in Figure 6a, and the blue spectrum in Figure 6c represents the sum of spectra from the dark regions in Figure 6a.

3.3. Further Spectroscopic Characteristics of Cu_xO_y. From the datasets shown so far, one cannot explicitly identify the atomic structure of the overlayer; so we gathered further spectroscopic data using in situ XPS and NEXAFS. Measurements were performed at 1×10^{-5} mbar O_2 and 300 °C. The Cu 2p photoemission spectrum of Cu_xO_y (Figure 7a) reveals a binding energy of 932.35 eV, which is nearly indistinguishable from Cu_2O (binding energy of 932.3 eV).[12] The Cu LMM Auger spectrum in Figure 7b, however, shows that the overlayer's Cu LMM characteristics are significantly different from all reference spectra (metallic copper, Cu_2O and CuO).[15] Furthermore, the O 1s spectrum of Cu_xO_y (binding energy of 529.5 eV) is between that of CuO and Cu_2O and is comparable with previous reports of O-terminated copper single crystal surfaces.[12] The Ag $3d_{5/2}$ binding energy of 368.2 eV is indistinguishable from metallic silver.[16]

The Cu L_3-edge NEXAFS spectrum reveals a very distinct feature of the Cu_xO_y structure (Figure 8a). While the lineshape resembles Cu_2O, the position of the absorption edge is shifted by 0.75 eV toward lower photon energy. This large shift implies a substantial difference in properties between Cu_xO_y and Cu_2O. To precisely determine the magnitude of this shift, we generated an internal standard by over-oxidized the sample (0.2 mbar O_2, 400 °C for 90 min) until bulk Cu_2O formed on the surface. This procedure allowed direct comparison of Cu_xO_y and Cu_2O (Figure 8a). As discussed in detail in the Supporting Information (see S4), the shift is a result of the lack of a band gap in Cu_xO_y. DFT calculations of the DOS show that the oxide is electronically coupled to the underlying metal, giving rise to states at the Fermi level. The O K-edge NEXAFS (Figure 8b) of Cu_xO_y resembles O-terminated Cu(111) surface, with features at 530.0 and 532.7 eV.[12] However, if an O-terminated Cu-surface were the correct interpretation of the structure, the Cu L_3-edge NEXAFS spectrum should resemble metallic copper, which it not the case. In summary, we observe an O K-edge that resembles O-terminated Cu, and a Cu L-edge that resembles Cu_2O, but with a substantial shift (Figure 8b).

4. DISCUSSION

4.1. Candidate Structures. Copper's affinity for oxygen gives rise to adsorbate-driven surface segregation.[17−21] Several oxides could potentially be formed. Previous ab-initio thermodynamics work identified three candidate structures likely formed on AgCu in an oxidizing atmosphere:[21] (I) a chemisorbed oxygen species (Figure 9a); (II) Cu_2O-like structures including two different candidates that are of particular interest: p2 (Figure 9b) and p4-OCu_3 (Figure 9c); and (III) a structure derived from CuO that we call CuO-1L (Figure 9d). The thermodynamic stability of these surface structures depends on both the oxygen chemical potential ($\Delta\mu_O$) and the Cu solute concentration in the bulk of AgCu(111).

Because of the inherent error of DFT-based calculations, one cannot definitively identify the structure solely by the calculated energy. While the chemisorbed structure (Cu_4O_4) is too high in energy to feasibly form, the p2 and p4-OCu_3 structures are predicted to be the most stable, with an almost degenerate Gibbs surface free energy.[10] Given the stability of these structures, and the fact that kinetics also plays a role in oxide formation, a variety of oxides could be expected to coexist, with a tendency to form bulk-like structures at higher Cu coverages and increasing $\Delta\mu_O$.[10]

The LEED patterns presented in Figures 4a and 5d strongly suggest a (2×2) periodicity of the overlayer with respect to the AgCu(111) surface. Hence, the (4×4) periodicity of the p4-OCu_3 structure is not observed, and we can discard this structure as a candidate. It should be emphasized that the p2 structure was proposed based on analogous systems (i.e. the "44" structure on Cu).[10] However, given the energy error inherent to DFT calculations, the subtle structural features, such as the pseudo-registry observed here, are difficult to predict.

4.2. Further Selection of Structure Candidates. While the spectroscopic similarities to Cu_2O suggests p2 or p4-OCu_3 as likely candidates, further confirmation was obtained by comparing the measured valence spectra with simulated spectra based on DFT calculated DOS. In order to compare with experimental photoemission spectra, the calculated pDOS were scaled by the respective computed gas-phase photoionization cross sections [σ(O 2p) = 0.292 and σ(Cu 3d) = 3.644 at the experimentally used photon energy of $h\nu$ = 170 eV]. An energy-dependent Lorentzian lifetime broadening was applied to the calculated DOS (0.003 eV broadening per eV). A three parameter Tougaard background was subtracted from the measured spectra to account for the inelastic scattering signal.

Figure 10a shows the measured spectra of Cu_2O and Cu_xO_y. One can see that Cu 3d band of Cu_xO_y is narrower than Cu_2O and is shifted toward higher binding energy. These same differences are reproduced by the DFT calculations of the p2 structure (Figure 10b). Not only are the peak position and the narrowness of the Cu 3d states well reproduced, so too are the observed shifts of the O 2p-related states (shoulder at ca. 1–2 eV).

Chemisorbed oxygen (Cu_4O_4) exhibits a somewhat similar Cu 3d peak shape to the p2 structure (except for the substantially larger intensity at 6–8 eV in the DOS of Cu_4O_4); however, Cu_4O_4 has a substantially higher energy than the p2 structure and is not considered a likely candidate for the observed phase.

Finally, the CuO-1ML structure exhibits a much broader feature in the valence band than seen for Cu_xO_y, similar to its structural analogue, bulk CuO. The increased band width is due to the strong hybridization of Cu 3d and O 2p states in CuO, giving rise to the feature at 4–6 eV.[15] From the partial DOS (Figure S5), one can see that the O states contribute more intensively over a wider energy range to the measurable photoemission signal as compared to the other candidate structures. The calculated DOS of the CuO-1ML structure candidate in combination with the absence of experimental evidence for Cu^{2+} in the Cu 2p core level spectrum (i.e. strong satellite structure) leads us to conclude that CuO-1ML is an unlikely candidate.

4.3. Structure Model. Based on the experimental evidence, the overlayer appears to be based on the p2 structure, however, with a subtle difference. As shown in Figure 5d, the LEED pattern of Cu_xO_y exhibits a Moiré pattern, suggesting that the overlayer is slightly incommensurate with

https://dx.doi.org/10.1021/acsami.0c03963
ACS Appl. Mater. Interfaces 2020, 12, 23595−23605

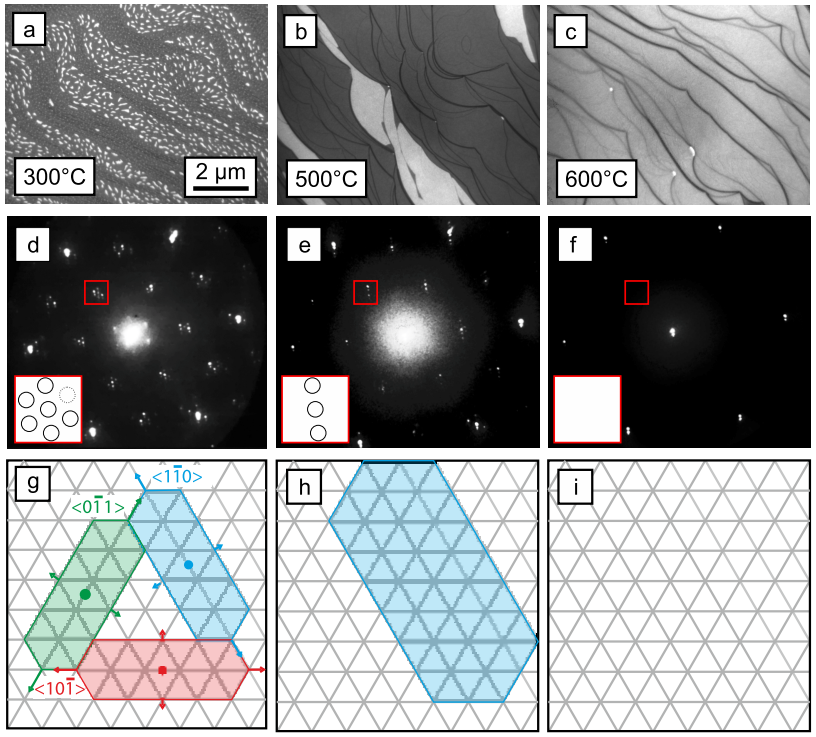

Figure 11. (a–c) LEEM images (E_{kin} = 16 eV) measured at increasing annealing temperatures in 1 × 10^{-5} mbar O_2. (d–f) Corresponding LEED patterns from the images in (a–c). (g–i) Lattice models illustrating how the Cu_xO_y islands nucleate, coalesce, and then decompose at increasing temperatures.

the Ag(111) surface. This observation could imply that the Cu_xO_y structure is either expanded or compressed in all directions parallel to the AgCu(111) surface. However, an interesting change occurs upon annealing. When annealed to 500 °C, the Cu_xO_y domains coalesce into larger patches, and the diffraction pattern changes (see Figure 11a,b), such that the Moiré spots no longer exhibit the three-fold symmetry of the substrate but rather a two-fold symmetry, as shown in Figure 11d,e. The fact that the Moiré pattern becomes 2-fold symmetric after annealing implies that the expansion/compression of the p2 lattice is actually only in one lattice direction and that the 6-fold Moiré pattern was a consequence of symmetry equivalent rotational domains.

Figure 11g–i depicts a structural model to explain the observed diffraction pattern changes with increasing temperatures. At 350 °C, three distinct rotational domains nucleate on the surface, each with a pseudo-(2 × 2) structure, expanded or compressed relative to the substrate by 8% in the ⟨1−10⟩ directions. The domains nucleate and grow until the fast-growing direction intersects a neighboring domain. When domains meet, growth in the fast direction stops and only proceeds in the perpendicular directions, but slower. This growth mechanism can explain the observed surface morphology and LEED patterns seen in Figure 5c,d. When the surface—kinetically stuck in this state—is annealed, the kinetic barriers of surface diffusion are overcome, and the overlayer recrystallizes, with Ostwald ripening giving rise to a few large dominant rotational domains, as depicted in Figure 11b.

Calculated Gibb's free energies of compressed and expanded p2 lattices, having superstructures of (12 × 2), (13 × 2), and (14 × 2) unit cell sizes relative to the Ag(111) surface (see Table S6), show that the 8% distortion is an expansion of the p2 lattice. The free energy minimum was found to be the (13 × 2) superstructure. An atomic model of the structure is shown in Figure 12. The Cu_2O-like lattice in the (13 × 2) structure

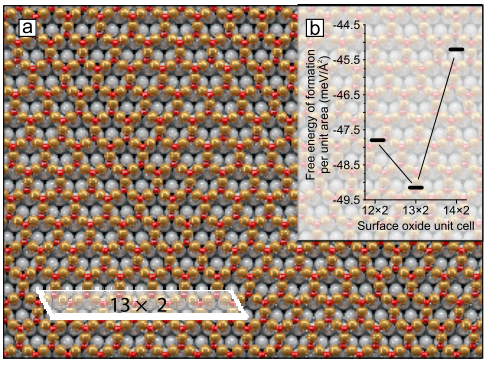

Figure 12. (a) Real space model of the overlayer oxide structure on the AgCu(111) surface. The (13 × 2) unit cell is indicated. (b) Calculated free energy of formation for three overlayer unit cells with varying amounts of expansion in one direction.

has a +4.1% strain in the ⟨0−11⟩ direction and a strain of −4.2% in the ⟨01−1⟩ direction, relative to bulk Cu_2O. With this pseudo-commensurate overlayer structure, Cu atoms of the overlayer are situated in several coordination sites of the substrate (i.e., hollow, bridge, and top sites). Calculations in which the p2 structure is translated across the Ag into various coordination sites show that Cu in the p2 structure has almost no preference for a coordination site (Table S7), indicating a very weak interaction between the overlayer oxide and the metal surface.

4.4. Electronic Structure of the 2D-Oxide. The majority of the experimental and theoretical data indicate that the chemical state of the proposed Cu_xO_y structure is similar to

https://dx.doi.org/10.1021/acsami.0c03963
ACS Appl. Mater. Interfaces 2020, 12, 23595−23605

that of Cu_2O. The measured Cu 2p binding energies presented in Figure 7a only differ by 0.05 eV compared to Cu_2O, and ground state DFT calculations show very similar initial-state energies of the two structures (Table S9). Moreover, Löwdin charge population analysis revealed both structures to have comparable charge densities (Table S10). However, the position of the Cu L-edge of the Cu_xO_y structure is significantly different from Cu_2O, with the absorption edge of Cu_xO_y being 0.75 eV lower than Cu_2O (Figure 8a). As elaborated in Supporting Information (see Figure S4), the reason for this shift is due to the lack of a band gap in the p2 structure when it is electronically coupled to the metallic substrate, as weak hybridization between the overlayer with the substrate gives rise to DOS across the Fermi level (see Figure S15). The white line shift seen in NEXAFS is not an indication of the charge on the Cu centers. In fact, all data suggest that the oxidation state of Cu in the p2 structure is very close to that of Cu in Cu_2O.

4.5. Comparison with Other Known Structures. There is a substantial body of knowledge about surface structures of Cu single crystals when exposed to low oxygen pressures.[22−28] In general, there are two types of structure: (1) non-oxide like and (2) oxide-like monolayers. The type-1 structures consist of O ions bound to the Cu surface, where the translational symmetry of the O lattice does not resemble the O-sub-lattice of any copper oxide. In contrast, the type-2 structures resemble a single lattice plane of Cu_2O and can be thought of as 2D oxides.[22,29,30] Because of the differences in the preferred Cu spacing of the oxide sub-lattice planes and the metallic Cu substrate, the oxide layers are quasi-epitaxial and exhibit interfacial strain with the underlying substrate.[25]

The Cu(100) and Cu(110) surfaces are only known to form type-1 structures. However, after large doses of oxygen, Cu_2O nucleates on the surfaces and exhibits 3D growth.[23,31] In contrast, the Cu(111) surface prefers to form an oxide-like 2D structure on its surface (with a meta-stable chemisorbed structure formed only within a narrow range of conditions).[25] The 2D oxide that forms on Cu(111) is structurally analogous to the (111) plane of bulk Cu_2O.

The preference for non-oxide-like versus oxide-like structures is driven by the Cu−O bond strength in the overlayer structure compared to the O-substrate bond strength. For the Cu(100) and Cu(110) surfaces, the Cu atoms are not very densely packed, allowing for a high coordination to O ions, and consequently strong Cu−O bonds. In contrast, the Cu(111) surface, which is densely packed, cannot provide high coordination to adsorbed O ions. Consequently, the Cu−O bond to the Cu(111) surface is comparatively weak, and the Cu−O bond in the 2D oxide is preferred.

To draw a comparison with the p2 structure on AgCu, O forms a weak bond with Ag and prefers to be in a coordination environment surrounded by Cu ions. This preference drives O and Cu to form the oxide-like surface structure rather than a chemisorbed structure. However, the superstructure of the 2D oxide on AgCu exhibits a unit cell 13 times larger than the Ag(111) repeating unit, and only distorted in one crystallographic direction while the oxide-like layers on Cu(111), such as the "29" and "44" structures, exhibit unit cells that are 29-times and 44-times larger than the Cu(111) repeating unit and are isotropic.

4.6. Relation to Ethylene Epoxidation. Previous works on ethylene epoxidation over silver catalysts have identified several adsorbed oxygen species present on Ag that could play a role in epoxidation[32−36] The identities of these species are still debated in the literature, but the hypothesized species include chemisorbed, ordered O-ions, chemisorbed disordered O-ions, sub-surface species, and species from common impurities, such as SiO_2 and SO_x.[35,37−41]

Under the conditions used in the present work to oxidize AgCu, some regions of the surface remained non-oxidized (as seen in Figure 4). These regions consist of metallic AgCu. The valence band spectra of these regions indicate that the metallic surface remains oxygen-free (there is no superstructure in the LEED pattern, and the valence band spectrum bears the signature of the clean alloy surface). Presumably, copper's much higher propensity for O compared to silver's caused any adsorbed O ions to be incorporated into the Cu_xO_y film.[21] However, at higher pressures, one would expect a more dynamic situation, where a steady-state population of adsorbed O species would develop on the metallic surface as well. Evidence of this assumption can be seen in the difference spectrum from NAP-XPS conditions of Figure 2B, where the metallic alloy spectrum exhibits some evidence of adsorbed O species (the feature at 1−2 eV). It is possible that at higher pressure, O ions could dynamically exchange between the Cu_xO_y film, metallic surface, and ethylene.

Whether or not the Cu_xO_y structure plays an active role in epoxidation is left up for debate, as a conclusive answer to this question is outside the scope of the present work. While the structure has previously been shown to be correlated with epoxide selectivity,[4] theoretical work has also shown that epoxidation on the p2 structure would have a quite high activation barrier (calculated using DFT to be 1.49 eV).[42] Alternatively, the oxide could work as a source or sink for adsorbed O-species on the metallic surface, giving rise to high population of selective O-species or decrease in population of non-selective O-species. Such a mechanism has been proposed to be the reason why small amounts of sulfur can enhance epoxide selectivity.[41] Furthermore, the decomposition of Cu_xO_y shown in the present work (Figure 11c) indicates that the 2D oxide is relatively unstable (compared to Cu_2O). Thus, it is quite possible that it plays an important role in populating the Ag surface with O ions.

5. CONCLUSIONS

We have experimentally determined that a two-dimensional meta-stable Cu_xO_y surface oxide forms on AgCu alloys under ethylene epoxidation conditions using a combination of in situ, model and theoretical experiments. The structure is in essence a lattice plane of Cu_2O placed on an Ag surface. It exhibits a copper oxidation state similar to Cu in Cu_2O; however, a weak coupling to the underlying metal affords its metallic properties. We thoroughly characterize the structure using XPEEM, LEED, UPS, XPS, and NEXAFS and compare the findings with DFT calculations. The structure is similar to the p2 structure previously predicted by Piccinin et al.[21] but exhibits a pseudo-commensurate relationship with the underlying metal, with a unidirectional 8% expansion, relative to the underlying substrate.

The current study showcases the need of combining a multitude of experimental and theoretical approaches to elucidate the structures of a meta-stable species formed in reactive environments. A systematic linking of experimental results, by means of common attributes to bridge the pressure and complexity gap between individual approaches, enables the

https://dx.doi.org/10.1021/acsami.0c03963
ACS Appl. Mater. Interfaces 2020, 12, 23595−23605

development of a valuable synergy between experiments and theory.

■ ASSOCIATED CONTENT

Supporting Information

The Supporting Information is available free of charge at https://pubs.acs.org/doi/10.1021/acsami.0c03963.

Sample preparation data, outline of how datasets are connected, schematic to accompany the explanation of the observed NEXAFS peak position for the surface structure, calculated projected DOS for all surface structures discussed, calculated surface energies of strained overlayer structure, XPS and LEEM data of the overlayer structure when cooled in liquid nitrogen, calculated XPS binding energies and charge integrations from Cu_2O, Cu and the p2 structure, explanation of the PCA procedure used in the main text, compilation of known O 1s binding energies for Ag−O and Cu−O systems, calculated projected DOS of a free-standing p2 film, and figure showing the lattice strain in 13 × 2 overlayer structure (PDF)

■ AUTHOR INFORMATION

Corresponding Authors

Kevin Schweinar − *Department of Microstructure Physics and Alloy Design, Max-Planck-Institut für Eisenforschung GmbH, 40237 Düsseldorf, Germany;* orcid.org/0000-0003-1595-2250; Email: k.schweinar@mpie.de

Mark T. Greiner − *Department of Heterogeneous Reactions, Max-Planck Institute for Chemical Energy Conversion, 45470 Mülheim an der Ruhr, Germany;* orcid.org/0000-0002-4363-7189; Email: mark.greiner@cec.mpg.de

Authors

Sebastian Beeg − *Department of Heterogeneous Reactions, Max-Planck Institute for Chemical Energy Conversion, 45470 Mülheim an der Ruhr, Germany*

Caroline Hartwig − *Department of Heterogeneous Reactions, Max-Planck Institute for Chemical Energy Conversion, 45470 Mülheim an der Ruhr, Germany*

Catherine R. Rajamathi − *Department of Heterogeneous Reactions, Max-Planck Institute for Chemical Energy Conversion, 45470 Mülheim an der Ruhr, Germany*

Olga Kasian − *Department of Interface Chemistry and Surface Engineering, Max-Planck-Institut für Eisenforschung GmbH, 40237 Düsseldorf, Germany; Helmholtz Zentrum Berlin für Materialien und Energie, 14109 Berlin, Germany;* orcid.org/0000-0001-6315-0637

Simone Piccinin − *CNR-IOM DEMOCRITOS, Istituto Officina dei Materiali, Consiglio Nazionale delle Ricerche, 34136 Trieste, Italy;* orcid.org/0000-0002-3601-7141

Mauricio J. Prieto − *Fritz-Haber-Institute of the Max-Planck Society, Department of Interface Science and Department of Chemical Physics, 14195 Berlin, Germany;* orcid.org/0000-0002-5087-4545

Liviu C. Tanase − *Fritz-Haber-Institute of the Max-Planck Society, Department of Interface Science and Department of Chemical Physics, 14195 Berlin, Germany;* orcid.org/0000-0002-4177-5676

Daniel M. Gottlob − *Fritz-Haber-Institute of the Max-Planck Society, Department of Chemical Physics, 14195 Berlin, Germany*

Thomas Schmidt − *Fritz-Haber-Institute of the Max-Planck Society, Department of Interface Science and Department of Chemical Physics, 14195 Berlin, Germany;* orcid.org/0000-0003-4389-2080

Dierk Raabe − *Department of Microstructure Physics and Alloy Design, Max-Planck-Institut für Eisenforschung GmbH, 40237 Düsseldorf, Germany*

Robert Schlögl − *Department of Heterogeneous Reactions, Max-Planck Institute for Chemical Energy Conversion, 45470 Mülheim an der Ruhr, Germany; Department of Inorganic Chemistry, Fritz-Haber Institute of the Max-Planck Society, 14195 Berlin, Germany*

Baptiste Gault − *Department of Microstructure Physics and Alloy Design, Max-Planck-Institut für Eisenforschung GmbH, 40237 Düsseldorf, Germany; Department of Materials, Imperial College London, Royal School of Mines, London SW7 2AZ, U.K.*

Travis E. Jones − *Department of Inorganic Chemistry, Fritz-Haber Institute of the Max-Planck Society, 14195 Berlin, Germany;* orcid.org/0000-0001-8921-7641

Complete contact information is available at: https://pubs.acs.org/10.1021/acsami.0c03963

Funding

Financial support by the Federal German Ministry of Education and Research (BMBF) under the contract 05 KS4WWB/4 as well as by the Max-Planck Society is gratefully acknowledged.

Notes

The authors declare no competing financial interest.

■ ACKNOWLEDGMENTS

The authors would like to thank HZB for the allocation of synchrotron radiation beamtime. K.S. is grateful for funding through the IMPRS-SurMat graduate school. Monika Nellessen and Katja Angenendt are acknowledged for their support in the metallography facilities at MPIE.

■ REFERENCES

(1) Norskov, J. K.; Abild-Pedersen, F.; Studt, F.; Bligaard, T. Density Functional Theory in Surface Chemistry and Catalysis. *Proc. Natl. Acad. Sci. U.S.A.* **2011**, *108*, 937−943.

(2) Nørskov, J. K.; Bligaard, T.; Rossmeisl, J.; Christensen, C. H. Towards the Computational Design of Solid Catalysts. *Nat. Chem.* **2009**, *1*, 37−46.

(3) Reuter, K.; Stampf, C.; Scheffler, M. Ab Initio Atomistic Thermodynamics and Statistical Mechanics of Surface Properties and Functions. In *Handbook of Materials Modeling: Methods*; Yip, S., Ed.; Springer Netherlands: Dordrecht, 2005; pp 149−194.

(4) Greiner, M. T.; Cao, J.; Jones, T. E.; Beeg, S.; Skorupska, K.; Carbonio, E. A.; Sezen, H.; Amati, M.; Gregoratti, L.; Willinger, M.-G.; Knop-Gericke, A.; Schlögl, R. Phase Coexistence of Multiple Copper Oxides on AgCu Catalysts during Ethylene Epoxidation. *ACS Catal.* **2018**, *8*, 2286−2295.

(5) Linic, S.; Jankowiak, J.; Barteau, M. A. Selectivity Driven Design of Bimetallic Ethylene Epoxidation Catalysts from First Principles. *J. Catal.* **2004**, *224*, 489−493.

(6) Jankowiak, J.; Barteau, M. Ethylene Epoxidation over Silver and Copper−Silver Bimetallic Catalysts: I. Kinetics and Selectivity. *J. Catal.* **2005**, *236*, 366−378.

(7) Schmidt, T.; Marchetto, H.; Lévesque, P. L.; Groh, U.; Maier, F.; Preikszas, D.; Hartel, P.; Spehr, R.; Lilienkamp, G.; Engel, W.; Fink, R.; Bauer, E.; Rose, H.; Umbach, E.; Freund, H.-J. Double Aberration

Correction in a Low-Energy Electron Microscope. *Ultramicroscopy* **2010**, *110*, 1358−1361.
(8) Schmidt, T.; Sala, A.; Marchetto, H.; Umbach, E.; Freund, H.-J. First Experimental Proof for Aberration Correction in XPEEM: Resolution, Transmission Enhancement, and Limitation by Space Charge Effects. *Ultramicroscopy* **2013**, *126*, 23−32.
(9) Krukau, A. V.; Vydrov, O. A.; Izmaylov, A. F.; Scuseria, G. E. Influence of the Exchange Screening Parameter on the Performance of Screened Hybrid Functionals. *J. Chem. Phys.* **2006**, *125*, 224106.
(10) Piccinin, S.; Stampfl, C.; Scheffler, M. Ag−Cu Alloy Surfaces in an Oxidizing Environment: A First-Principles Study. *Surf. Sci.* **2009**, *603*, 1467−1475.
(11) Giannozzi, P.; Baroni, S.; Bonini, N.; Calandra, M.; Car, R.; Cavazzoni, C.; Ceresoli, D.; Chiarotti, G. L.; Cococcioni, M.; Dabo, I.; Dal Corso, A.; de Gironcoli, S.; Fabris, S.; Fratesi, G.; Gebauer, R.; Gerstmann, U.; Gougoussis, C.; Kokalj, A.; Lazzeri, M.; Martin-Samos, L.; Marzari, N.; Mauri, F.; Mazzarello, R.; Paolini, S.; Pasquarello, A.; Paulatto, L.; Sbraccia, C.; Scandolo, S.; Sclauzero, G.; Seitsonen, A. P.; Smogunov, A.; Umari, P.; Wentzcovitch, R. M. QUANTUM ESPRESSO: A Modular and Open-Source Software Project for Quantum Simulations of Materials. *J. Phys.: Condens. Matter* **2009**, *21*, 395502.
(12) Greiner, M. T.; Jones, T. E.; Johnson, B. E.; Rocha, T. C. R.; Wang, Z. J.; Armbrüster, M.; Willinger, M.; Knop-Gericke, A.; Schlögl, R. The Oxidation of Copper Catalysts During Ethylene Epoxidation. *Phys. Chem. Chem. Phys.* **2015**, *17*, 25073−25089.
(13) Hüfner, S.; Wertheim, G. K.; Smith, N. V.; Traum, M. M. XPS Density of States of Copper, Silver, and Nickel. *Solid State Commun.* **1972**, *11*, 323−326.
(14) Schön, G. ESCA Studies of Cu, Cu_2O and CuO. *Surf. Sci.* **1973**, *35*, 96−108.
(15) Ghijsen, J.; Tjeng, L. H.; van Elp, J.; Eskes, H.; Westerink, J.; Sawatzky, G. A.; Czyzyk, M. T. Electronic Structure of Cu_2O and CuO. *Phys. Rev. B* **1988**, *38*, 11322−11330.
(16) Kaushik, V. K. XPS Core Level Spectra and Auger Parameters for some Silver Compounds. *J. Electron Spectrosc. Relat. Phenom.* **1991**, *56*, 273−277.
(17) Skriver, H. L.; Rosengaard, N. M. Surface Energy and Work Function of Elemental Metals. *Phys. Rev. B* **1992**, *46*, 7157−7168.
(18) Herron, J. A.; Mavrikakis, M. On the Composition of Bimetallic Near-Surface Alloys in the Presence of Oxygen and Carbon Monoxide. *Catal. Commun.* **2014**, *52*, 65−71.
(19) Kitchin, J. R.; Reuter, K.; Scheffler, M. Alloy Surface Segregation in Reactive Environments: First-Principles Atomistic Thermodynamics Study of $Ag_3Pd(111)$ in Oxygen Atmospheres. *Phys. Rev. B* **2008**, *77*, 075437.
(20) Han, B. C.; Van der Ven, A.; Ceder, G.; Hwang, B.-J. Surface Segregation and Ordering of Alloy Surfaces in the Presence of Adsorbates. *Phys. Rev. B* **2005**, *72*, 205409.
(21) Piccinin, S.; Stampfl, C.; Scheffler, M. First-Principles Investigation of Ag-Cu Alloy Surfaces in an Oxidizing Environment. *Phys. Rev. B* **2008**, *77*, 075426.
(22) Gattinoni, C.; Michaelides, A. Atomistic Details of Oxide Surfaces and Surface Oxidation: The Example of Copper and its Oxides. *Surf. Sci. Rep.* **2015**, *70*, 424−447.
(23) Lahtonen, K.; Hirsimäki, M.; Lampimäki, M.; Valden, M. Oxygen Adsorption-Induced Nanostructures and Island Formation on Cu{100}: Bridging the Gap Between the Formation of Surface Confined Oxygen Chemisorption Layer and Oxide Formation. *J. Chem. Phys.* **2008**, *129*, 124703.
(24) Judd, R. W.; Hollins, P.; Pritchard, J. The Interaction of Oxygen with Cu(111): Adsorption, Incorporation and Reconstruction. *Surf. Sci.* **1986**, *171*, 643−653.
(25) Wiame, F.; Maurice, V.; Marcus, P. Initial Stages of Oxidation of Cu(111). *Surf. Sci.* **2007**, *601*, 1193−1204.
(26) Moritani, K.; Okada, M.; Teraoka, Y.; Yoshigoe, A.; Kasai, T. Reconstruction of Cu(111) Induced by a Hyperthermal Oxygen Molecular Beam. *J. Phys. Chem. C* **2008**, *112*, 8662−8667.
(27) Matsumoto, T.; Bennett, R. A.; Stone, P.; Yamada, T.; Domen, K.; Bowker, M. Scanning Tunneling Microscopy Studies of Oxygen Adsorption on Cu(111). *Surf. Sci.* **2001**, *471*, 225−245.
(28) Jensen, F.; Besenbacher, F.; Stensgaard, I. Two New Oxygen Induced Reconstructions on Cu(111). *Surf. Sci.* **1992**, *269-270*, 400−404.
(29) Soon, A.; Todorova, M.; Delley, B.; Stampfl, C. Surface Oxides of the Oxygen−Copper System: Precursors to the Bulk Oxide Phase? *Surf. Sci.* **2007**, *601*, 5809−5813.
(30) Soon, A.; Todorova, M.; Delley, B.; Stampfl, C. Oxygen Adsorption and Stability of Surface Oxides on Cu(111): A First-Principles Investigation. *Phys. Rev. B* **2006**, *73*, 165424.
(31) Duan, X.; Warschkow, O.; Soon, A.; Delley, B.; Stampfl, C. Density Functional Study of Oxygen on Cu(100) and Cu(110) Surfaces. *Phys. Rev. B* **2010**, *81*, 075430.
(32) Williams, F. J.; Bird, D. P. C.; Palermo, A.; Santra, A. K.; Lambert, R. M. Mechanism, Selectivity Promotion, and New Ultraselective Pathways in Ag-Catalyzed Heterogeneous Epoxidation. *J. Am. Chem. Soc.* **2004**, *126*, 8509−8514.
(33) Su, D. S.; Jacob, T.; Hansen, T. W.; Wang, D.; Schlögl, R.; Freitag, B.; Kujawa, S. Surface Chemistry of Ag Particles: Identification of Oxide Species by Aberration-Corrected TEM and by DFT Calculations. *Angew. Chem., Int. Ed.* **2008**, *47*, 5005−5008.
(34) Xu, Y.; Greeley, J.; Mavrikakis, M. Effect of Subsurface Oxygen on the Reactivity of the Ag(111) Surface. *J. Am. Chem. Soc.* **2005**, *127*, 12823−12827.
(35) Bukhtiyarov, V.; Nizovskii, A.; Bluhm, H.; Havecker, M.; Kleimenov, E.; Knopgericke, A.; Schlogl, R. Combined in situ XPS and PTRMS Study of Ethylene Epoxidation over Silver. *J. Catal.* **2006**, *238*, 260−269.
(36) Bukhtiyarov, V. I.; Hävecker, M.; Kaichev, V. V.; Knop-Gericke, A.; Mayer, R. W.; Schlögl, R. Atomic Oxygen Species on Silver: Photoelectron Spectroscopy and X-Ray Absorption Studies. *Phys. Rev. B* **2003**, *67*, 235422.
(37) Rocha, T. C. R.; Oestereich, A.; Demidov, D. V.; Hävecker, M.; Zafeiratos, S.; Weinberg, G.; Bukhtiyarov, V. I.; Knop-Gericke, A.; Schlögl, R. The Silver−Oxygen System in Catalysis: New Insights by Near Ambient Pressure X-ray Photoelectron Spectroscopy. *Phys. Chem. Chem. Phys.* **2012**, *14*, 4554−4564.
(38) Carlisle, C. I.; Fujimoto, T.; Sim, W. S.; King, D. A. Atomic Imaging of the Transition between Oxygen Chemisorption and Oxide Film Growth on Ag{111}. *Surf. Sci.* **2000**, *470*, 15−31.
(39) Bare, S. R.; Griffiths, K.; Lennard, W. N.; Tang, H. T. Generation of Atomic Oxygen on Ag(111) and Ag(110) using NO_2: A TPD, LEED, HREELS, XPS and NRA Study. *Surf. Sci.* **1995**, *342*, 185−198.
(40) Campbell, C. T. Atomic and Molecular Oxygen Adsorption on Ag(111). *Surf. Sci.* **1985**, *157*, 43−60.
(41) Jones, T. E.; Wyrwich, R.; Böcklein, S.; Carbonio, E. A.; Greiner, M. T.; Klyushin, A. Y.; Moritz, W.; Locatelli, A.; Menteş, T. O.; Niño, M. A.; Knop-Gericke, A.; Schlögl, R.; Günther, S.; Wintterlin, J.; Piccinin, S. The Selective Species in Ethylene Epoxidation on Silver. *ACS Catal.* **2018**, *8*, 3844−3852.
(42) Piccinin, S.; Nguyen, N. L.; Stampfl, C.; Scheffler, M. First-Principles Study of the Mechanism of Ethylene Epoxidation over Ag−Cu Particles. *J. Mater. Chem.* **2010**, *20*, 10521−10527.

https://dx.doi.org/10.1021/acsami.0c03963
ACS Appl. Mater. Interfaces 2020, 12, 23595−23605